Temperature Sensing Diode in InP-Based Photonic Integration Technology

Wenjing Tian, Bart Bas, Dylan Harmsen, Kevin Williams, and Xaveer Leijtens, *Senior Member, IEEE*

***Abstract*—The integration of temperature sensors directly onto photonic platforms facilitates the thermal management of advanced photonic integrated circuits. This paper presents monolithic temperature sensors on the indium-phosphide-based photonic integration technology. Two distinct sensors were developed using p-i-n diode junctions with different waveguide core layers, one composed of multiple quantum wells and the other of bulk indium gallium arsenide phosphide. Introducing these sensors to an indium-phosphide-based generic foundry platform required zero process modifications. Theoretical, simulation, and measurement results consistently reveal a linear relationship between the forward voltage of the sensors and temperature under constant current biasing. The measurement results highlight that the compact sensors with dimensions of 30 $\times$ 10 μm achieve the highest sensitivity of -2.1 mV/K. These sensors boast a simple structure, easy operation, straightforward temperature interpretation, and high compatibility with the foundry process. They present immunity to on-chip (stray) light, a critical feature when operating alongside integrated lasers. The results demonstrate the feasibility of local temperature measurement and monitoring of photonic integrated circuits.**

***Index Terms*—Diodes, photonic integrated circuits, temperature sensor, thermal management.**

I. Introduction

PHOTONIC integrated circuits (PICs), extensively explored in research, hold the potential for applications across diverse fields, such as high-speed transceivers in optical communications [1], integrated photonic switches in data centers and high-performance computing systems [2], and dense optical phased arrays for precise sensing and ranging [3]. Temperature plays a critical role in the performance and reliability of PICs [4], particularly within high-performance PICs that contain optical amplifiers, arrayed waveguide gratings, or lasers. In this context, temperature sensing has become a fundamental requirement for advanced photonic devices and systems. The continuous drive towards ever-higher performance and miniaturization demands efficient thermal management to ensure the stable operation of these PICs [5], [6]. A promising approach to address this growing demand involves the direct integration of temperature sensors on PICs. These integrated temperature sensors enable localized temperature measurement in proximity to the on-chip heat sources or temperature-sensitive components. Besides that, they facilitate temperature control in photonic modules that house packaged PICs. As the modules become more complex and compact, effective thermal management becomes critical to ensure optimal performance and reliability [7], [8], [9]. Integrated temperature sensors offer the capability to conduct localized temperature monitoring at multiple locations on the chips, eliminating the necessity for cumbersome off-chip temperature sensors.

Various types of integrated temperature sensors have been explored on photonic integration platforms such as Michelson interferometers [10], ring resonators [11], waveguide Bragg gratings [12], and photonic crystals [13]. These devices were initially developed to serve different functions, including optical interferometry, signal filtering, and wavelength-specific reflection. Operating such devices as temperature sensors requires external tunable lasers and optical spectrum analyzers, which brings complexity, hinders the achievement of higher integration density, and incurs higher costs. To eliminate the need for external optical sources and wavemeters, a diode-based temperature sensor offers a promising alternative [14]. The basic principle of detecting temperature is based on the diode current-voltage (I-V) characteristics, [14], [15]. The diode-based sensors provide a linear relationship between voltage and temperature when forward-biased at a constant current [14], [15], [16], [17], [18]. This linearity simplifies the calibration and interpretation of temperature measurements. In addition, diode-based temperature sensors offer advantages such as simple structure and easy operation.

Integrated diodes as on-chip temperature sensors have been theoretically studied, proven feasible, and found extensive application in electronic integrated circuits in complementary metal-oxide-semiconductor (CMOS) technology [15], [17], [18], [19], [20], [21]. These sensors operate within a temperature range that theoretically spans from -100 to 300 °C, and in practical terms, from -55 to 150 °C [14]. This practical range is chosen for improved linearity and alignment with the typical operating temperature range of electronic integrated circuits [18]. The typical sensitivity of these sensors varies from -1.2 to -2.2 mV/K, depending on forward-bias currents [15], [16], [17], [18], [22]. However, in the photonic domain, the investigation into the use of diodes as integrated temperature sensors has been limited primarily to leveraging silicon-based p-n junctions for thermal stabilization in silicon micro-ring modulators in photonic bipolar CMOS (BiCMOS) technology [23], [24], [25], [26]. These silicon-based diodes cannot be monolithically integrated

Manuscript received 27 December 2023; revised 16 February 2024; accepted 2 March 2024. Date of publication 6 March 2024; date of current version 4 April 2024. This work was supported in part by the European Union through Eurostars FLEXFIX Program nr. 2018.29, and in part by Microsoft Research through its Ph.D. Scholarship Programme. *(Corresponding author: Wenjing Tian.)*

The authors are with the Eindhoven Hendrik Casimir Institute, Eindhoven University of Technology, 5600MB Eindhoven, The Netherlands (e-mail: w.tian1@tue.nl).

Digital Object Identifier 10.1109/JPHOT.2024.3374266

into InP-based photonic integrated circuits due to different fabrication processes. The possibility of utilizing InP-based diodes as integrated temperature sensors in InP-based photonic integration technology has not yet been explored.

In this work, integrated temperature sensors based on InP p-i-n diodes were developed from building blocks offered in standard multi-project wafer (MPW) runs provided by the InP-based generic foundry SMART Photonics [27], [28]. Such sensors do not require changes in the fabrication process, except for modifications at the mask design level. Temperature sensing measurements were conducted by detecting variations in voltage at different temperatures when applying a constant current to the sensors. These sensors demonstrated resilience to the impact of on-chip light. The preliminary concept, design, and characterization results of the sensors were briefly outlined in previous works [29], [30]. This paper, for the first time to the best of our knowledge, extends this exploration by investigating the feasibility of employing InP p-i-n diodes as integrated temperature sensors in InP-based generic photonic integration technology through theoretical analysis, simulations, design considerations, and experiments.

II. Principle of Temperature Sensing Diodes

The concept of employing a p-n junction or bipolar junction transistor as a temperature sensor was initially introduced by McNamara in 1962 [22], with a thorough explanation of their operation principle provided by Meijer [16]. For an ideal diode, the current I through the p-n junction is given by the Shockley diode equation as [31]:

$$I = I_s(T)\left[\exp\left(\frac{qV}{nkT}\right) - 1\right], \tag{1}$$

where $I_s(T)$ is the saturation current (temperature dependent), q is the elemental charge, V is the forward voltage across the diode, n is the ideality factor, k is the Boltzmann constant, and T is the temperature. Note that $I_s(T)$ can be expressed as [14], [15], [16]:

$$I_s(T) = CT^{\eta}\exp\left(\frac{-qV_g}{kT}\right), \tag{2}$$

where C and η are constants that are independent of temperature. C is related to factors such as the density of states, effective masses of electrons and holes, carrier mobility, and physical parameters of the junction [14], [15], [16]. η depends on the process and slightly relates to the doping level, for example, the typical value of η for silicon is 3.5 [15], [18]. V_g represents the band gap voltage. The Shockley diode (1) can be rewritten to:

$$V = \frac{nkT}{q}\ln\left(\frac{I}{I_s(T)} + 1\right). \tag{3}$$

Substituting (2) into (3) gives:

$$V(T) = nV_g - \frac{n\eta kT}{q}\ln T + \frac{nkT}{q}\ln\frac{I}{C} + \frac{nkT}{q}\ln\left(\frac{I_s(T)}{I} + 1\right). \tag{4}$$

To deduce the voltage-temperature (V-T) relationship, two temperatures are considered: an arbitrary temperature T and a specified reference temperature T_r. The corresponding voltages $V(T)$ and $V(T_r)$ can be expressed using (4). Both expressions contain the same term $\ln(\frac{I}{C})$, enabling substituting the one in the other, which gives:

$$V(T) = n\left(V_g + \frac{\eta kT_r}{q}\right) - \frac{n\left(V_g + \frac{\eta kT_r}{q}\right) - V(T_r)}{T_r}T + \frac{n\eta k}{q}\left(T - T_r - T\ln\frac{T}{T_r}\right) + \frac{nkT}{q}\ln\left(\frac{I + I_s(T)}{I + I_s(T_r)}\right). \tag{5}$$

Here, the first term is a constant; the second term is linearly proportional to temperature, T; and the last two terms represent the non-linear part. The temperature gradient, $\frac{dV(T)}{dT}$, is defined to be the sensitivity of a diode temperature sensor. Provided that the saturation current I_s is significantly less than the bias current I, the sensitivity is given by [15], [16], [18]:

$$\frac{dV(T)}{dT} = -\left[n\left(V_g + \frac{\eta kT_r}{q}\right) - V(T_r)\right]\frac{1}{T_r}, \tag{6}$$

where the parameters n, V_g, η, k, q, and T_r are all considered temperature-independent constants. Neglecting the slight temperature dependence of V_g is validated by simulation and measurement results in the following sections, which demonstrate a (near) linear relationship between temperature and voltage when the diode is biased at a constant current. Besides these constants, the sensitivity further depends on the bias current I, considering $V(T_r)$ varies with this current, as indicated by (3). Therefore, a higher forward current will result in a lower absolute value of sensitivity (i.e., $|\frac{dV(T)}{dT}|$). Besides that, a high forward current will also introduce self-heating of the sensor through the parasitic series resistance of the diode. A typical sensitivity ranges from -1 to -3 mV/K [14].

III. Sensor Design

The design of temperature sensing diodes within InP-based generic photonic integration technology leverages the existing p-i-n diodes of the technology. Two types of p-i-n diodes are available on the InP-based MPW platform used in this study [27], [28]. These diodes both comprise a 500-nm-thick intrinsic layer as a waveguide core, with one version containing multiple (four) quantum wells (Q1.55-MQW) [27] and the other using lattice-matched Q1.25 bulk indium gallium arsenide phosphide (InGaAsP), illustrated in Fig. 1(b) and (c). Here, Q1.55 and Q1.25 denote different InGaAsP compositions with emitting wavelengths of 1550 nm and 1250 nm, respectively. On the InP-based MPW platform, the Q1.55-MQW and Q1.25-bulk diodes are employed as basic building blocks, specifically for semiconductor optical amplifiers (SOAs) and electro-refractive phase modulators, respectively [27].

Considering that the principle of temperature sensing diodes, as discussed earlier, was established for p-n diodes adhering to the Shockley model, the initial assessment of the InP-based p-i-n diodes focused on the diode characteristics and temperature

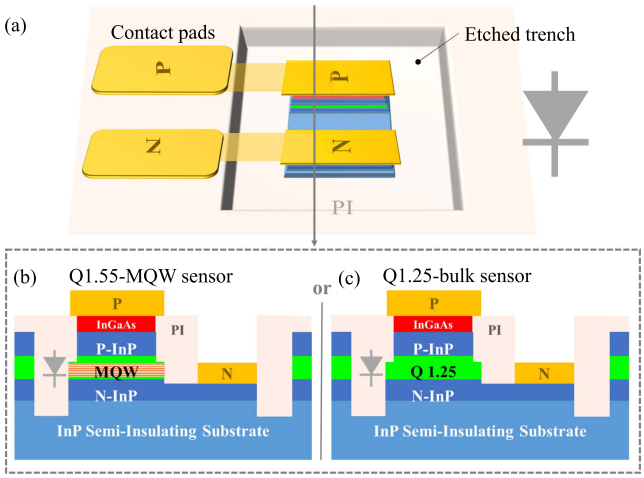

Fig. 1. (a) 3D schematic of a temperature sensing diode in the InP-based generic integration technology. Simplified cross-sectional views of (b) the Q1.55-MQW sensor and (c) the Q1.25-bulk sensor. PI: polyimide.

dependency. Simulations were performed using the program Harold, a hetero-structure simulator from Photon Design [32]. This software employs electromagnetic and quantum physics models to calculate the behavior and performance of diodes for a user-defined layer stack [32]. In the simulations, the layer stacks of both sensors (Fig. 1) were constructed. For a range of set temperatures, the I-V characteristics of both structures were simulated. Linear interpolation was applied to extract the V-T relationships under different conditions of forward-bias current densities. The sensitivities, $\frac{dV(T)}{dT}$, were determined using the slopes obtained from linear fits to the linear range of the V-T curves.

As depicted in Fig. 2(a) and (b), simulation results demonstrate that both sensors exhibit a (near) linear relationship between the forward voltage and temperature across the range of 0 to 200 °C. It can be seen that the two types of sensors differ in forward voltage and sensitivity. The Q1.55-MQW sensor exhibits lower forward voltages compared to the Q1.25-bulk sensor when driven at the same current densities. This voltage difference is attributed to their layer stack differences. Fig. 2(c) shows that the sensitivity of the Q1.55-MQW sensor varies from -1.9 to -1.0 mV/K, for current densities ranging from 0.01 to 10 A/cm^2. Higher sensitivities were observed for the Q1.25-bulk sensor, ranging from -2.1 to -1.5 mV/K for the same current range. The sensitivity difference between the two types of sensors is primarily attributed to the difference in their band gap voltage V_g, as indicated by (6). Therefore the Q1.25-bulk sensor has a higher sensitivity than the Q1.55-MQW sensor. There exists a trade-off between sensitivity and the linear range that is directly influenced by the forward-bias currents. When operating at lower forward-bias currents, the linear temperature range decreases, however, the sensitivity is enhanced, and self-heating is minimized.

Based on the theory and simulation results, several diode temperature sensors were designed in the InP-based generic photonic integration technology. As illustrated in Fig. 1, the sensors feature a junction positioned within an etched trench and

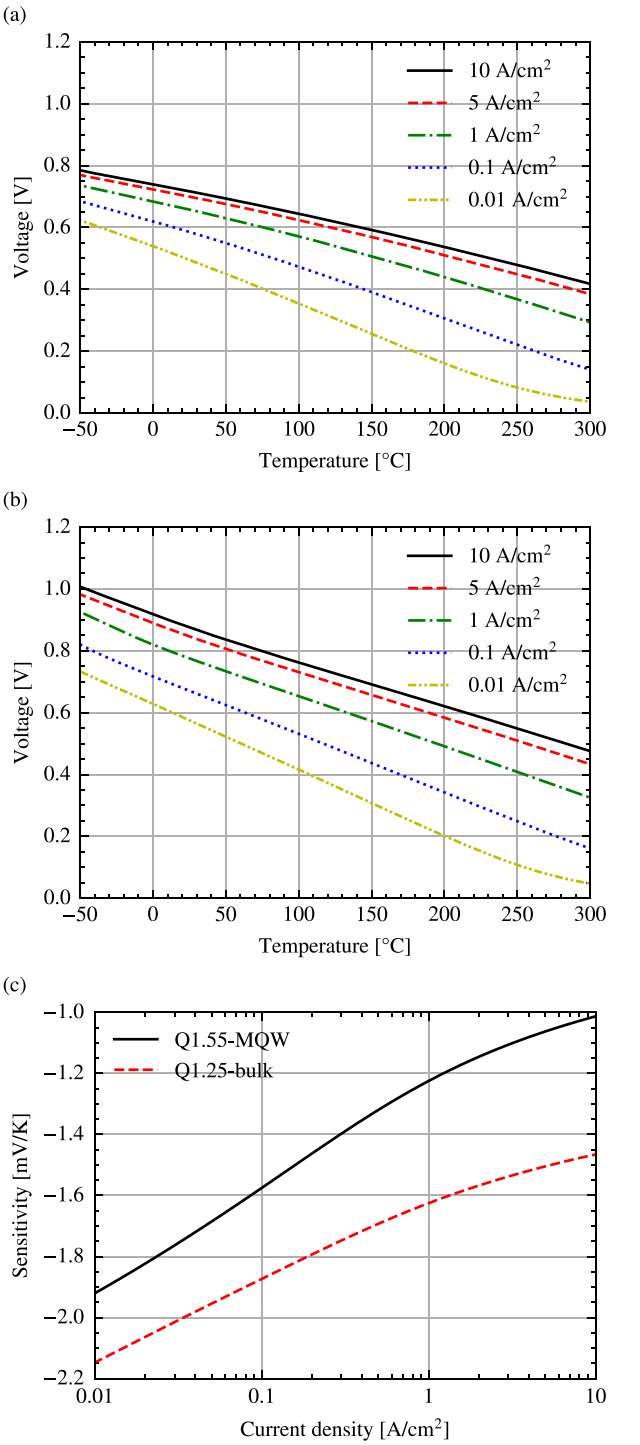

Fig. 2. Simulation results. The V-T relationship of both sensor types, (a) Q1.55-MQW and (b) Q1.25-bulk, over a temperature range of -50 to 300 °C for different forward-bias current densities. (c) sensitivities of the sensors calculated with a linear fit to the V-T curves between 0 and 200 °C.

two contact pads (gold-based) for electrical probing. The diode junction dimensions are 60 × 20 μm and 30 × 10 μm. The two contact pads measure 70 × 90 μm. The trench is employed to minimize leakage currents and reduce the impact of scattered light from neighboring electro-optic devices to the sensors. The sensors were fabricated through an MPW run offered by SMART

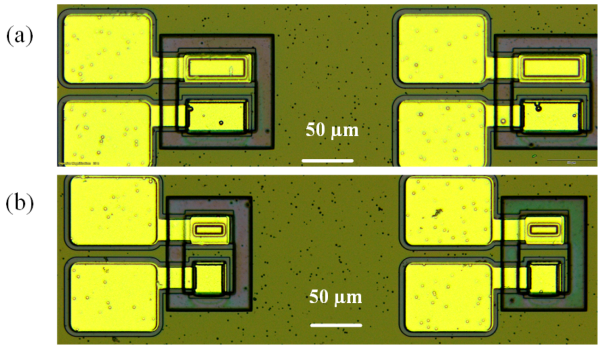

Fig. 3. Microscope images of four diode temperature sensors with dimensions of (a) 60 × 20 μm and (b) 30 × 10 μm. The left ones are Q1.55-MQW sensors and the right ones are Q1.25-bulk sensors.

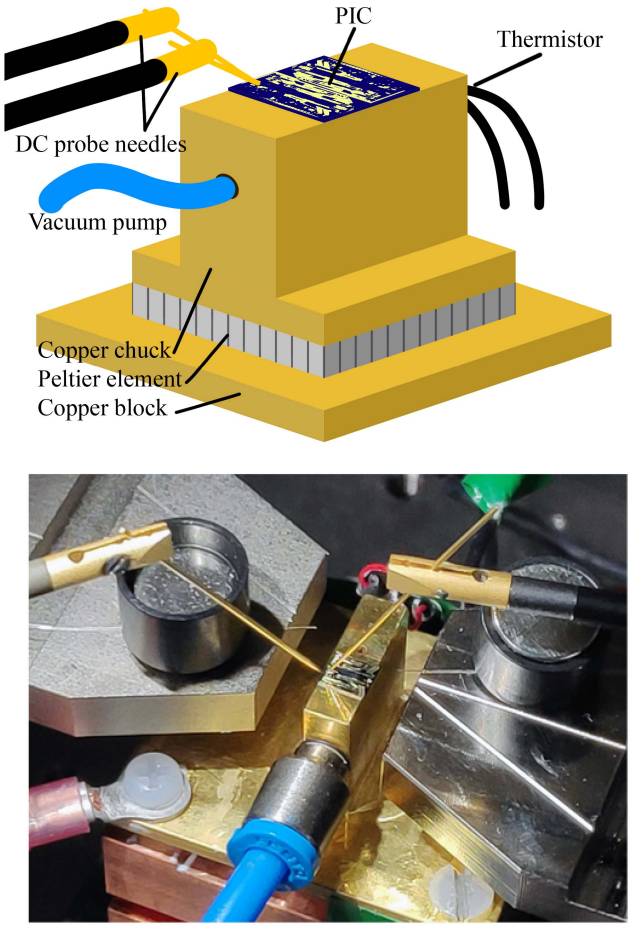

Fig. 4. Schematic (top) and photograph (bottom) illustrating the measurement setup and a PIC.

Photonics [27], via the JePPIX platform [33]. Fig. 3 shows microscope images of four fabricated diode temperature sensors.

IV. Measurement Results

A. Diode Characteristics

The measurement setup used to obtain the I-V characteristics and temperature dependency of the sensors is shown in Fig. 4. The PIC, containing the diode temperature sensors, was

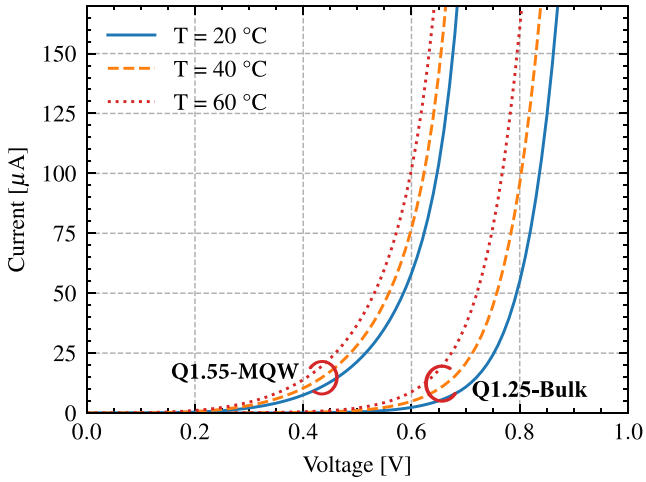

Fig. 5. Measurement results of I-V characteristics of InP p-i-n diodes (Q1.55-MQW and Q1.25-bulk sensors) at different temperatures of 20, 40, and 60 °C. The sensors have a junction area of 60 × 20 μm.

positioned on a chip holder constructed of two copper blocks (served as heat sinks) that have a thermo-electric cooler (TEC) sandwiched between them. The TEC controlled the overall temperature of the chip holder, which was monitored by an off-chip negative temperature coefficient (NTC) thermistor. The thermistor was inserted in the chip holder as a reference temperature sensor of the overall temperature. The TEC and thermistor were controlled by a TEC controller (Thorlabs PRO8000 TED8040) with built-in feedback control and calibration circuits. A source meter (Keithley 2602B) was employed to supply the current through the sensors and measure the corresponding voltage, and vice versa.

The I-V forward characteristics of the InP p-i-n diodes were initially measured at different temperatures of 20, 40, and 60 °C. The measurement results for these diodes (60 × 20 μm) at these temperatures are depicted in Fig. 5. The temperature was measured using the NTC thermistor as a reference sensor, illustrated in Fig. 4. As depicted in Fig. 5, the forward voltage of the diodes decreases with an increase in temperature when the diodes are biased at the same current level. The Q1.25-bulk sensor exhibits higher voltages compared to the Q1.55-MQW sensor, a trend also observed in the simulation results shown in Fig. 2.

V-T measurements were conducted on four variants of diodes, distinguished by their layer stack (Q1.25-bulk and Q1.55-MQW) and junction area (60 × 20 μm and 30 × 10 μm). Forward-bias current densities ranging from 0.8 to 10 A/cm^2 were used in the measurements. Using low current densities aimed to minimize self-heating effects. These measurements were carried out over a temperature range spanning from 16 to 60 ° C. This temperature range was chosen by practical considerations, including setup limitations and lab environment factors such as condensation. This chosen range aligns with typical operating scenarios for PICs. However, simulation results in Fig. 2 indicate that the sensors can be operated over a wider temperature range.

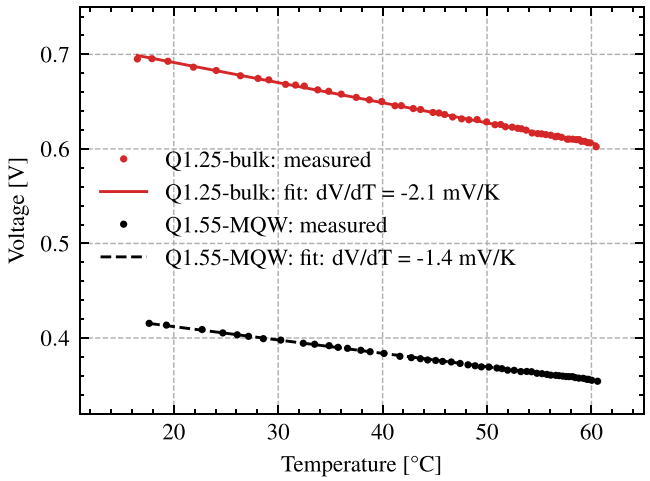

Fig. 6. Measurement results of the V-T relationship of Q1.55-MQW and Q1.25-bulk sensors, biased at a current density of 0.8 A/cm^2, over a temperature range of 16 - 60 ° C. The sensors have a junction area of 60 × 20 μm.

TABLE I
MEASUREMENT RESULTS OF THE V-T RELATIONSHIP

Junction area (μm^2)	Current density (A/cm^2)	Sensitivity (mV/K)	Power consumption (μW)
Q1.55-MQW sensor			
60×20	0.8	−1.4	3.8
60×20	5	−1.3	36.2
60×20	10	−1.1	78.8
30×10	1.7	−1.4	2.4
30×10	5	−1.4	8.6
30×10	10	−1.3	19.0
Q1.25-bulk sensor			
60×20	0.8	−2.1	6.4
60×20	5	−1.9	48.6
60×20	10	−1.8	101.5
30×10	1.9	−2.1	4.2
30×10	5	−1.9	11.1
30×10	10	−1.8	24.0

Note that the sensitivities were calculated by applying linear regression to the data from V-T measurements. The power consumption was obtained by multiplying the bias current and forward voltage at 20 °C.

Fig. 6 illustrates the measured V-T relationship for both sensors biased at the same current density of 0.8 A/cm^2. The measurement results demonstrate differences between the two sensor types in terms of forward voltage and sensitivity, primarily attributed to differences in the layer stack and band gap, which agree with simulation findings. The Q1.25-bulk sensor required higher forward voltages compared to the Q1.55-MQW sensor. Following a linear fit, the sensitivity of the sensors is found to be −2.1 mV/K for the Q1.25-bulk sensor, and −1.4 mV/K for the Q1.55-MQW sensor. The Q1.25-bulk sensor showed a higher sensitivity compared to the Q1.55-MQW sensor, aligning with simulation results. The V-T relationship remained consistent for the other current densities.

Further V-T measurement results are shown in Table I, including calculated sensitivities and power consumption of these sensors at 20 °C. As anticipated by the simulations, a lower current density offered an enhanced sensitivity, although the difference is minor. Another way to increase the sensitivity is by placing multiple diodes in series [18]. Moreover, a reduction in junction area resulted in a decreased bias current requirement at the same current density, leading to a corresponding decrease in power consumption. For instance, when biased at the same current density of 5 A/cm^2, a Q1.55-MQW sensor with a dimension of 30 × 10 μm exhibited a power consumption of 8.6 μW, which is lower than the 36.2 μW consumed by the larger 60 × 20 μm sensor. However, power consumption is not a major concern, because the sensor is only biased for a short time during a temperature measurement.

Additional V-T measurements were conducted on sensors on different PICs (dies) originating from various locations on the wafer in an MPW run (SI10). Furthermore, sensors with identical layer stacks to those demonstrated in this work, but differing in dimensions and lacking the etched trench surrounding the p-i-n junctions, were measured and evaluated on different PICs fabricated in two other MPW runs (SP20 and SP22) offered by SMART Photonics foundry. Consistently, these measurements showed the same linear voltage-temperature relation and similar sensitivities to the sensors demonstrated in this work. These results provide further evidence of the uniformity and consistency of the diode temperature sensors.

B. Sensor Response to On-Chip Light

The sensors have the potential to exhibit sensitivity to on-chip (stray) light, given the sensors are based on waveguide layer stacks, as depicted in Fig. 1. This possibility arises when they are exposed to light that is partly confined within the waveguides and partly leaks through the substrate of the surrounding devices. One example is light emitted from lasers on the same PIC. This exposure may induce fluctuations in diode voltages, potentially leading to wrong temperature measurements. To assess the extent of this influence, measurements were performed on the PIC featuring temperature sensors co-integrated with a semiconductor laser.

Fig. 7 shows the microscope image of two different sensors that were integrated alongside a semiconductor laser circuit in a shared design cell. This laser was used as a combined light and heat source to check the impact on the temperature sensors. The laser circuit consists of a 500-μm-long SOA and three phase shifters integrated into a race-track ring resonator. The L-I-V characteristics of the laser are shown in Fig. 8. The characteristics were measured at a stabilized temperature of 18 °C controlled by the TEC, using the setup shown in Fig. 4. The laser had a turn-on voltage of 0.7 V, and a threshold current of 37 mA (3.7 kA/cm^2). In addition, the series resistance was calculated to be 16 Ω based on the slope of the V-I curve at 18 °C. The output power of the laser was 0.3 mW (coupled into an optical fiber) when the laser was biased at 80 mA (8.0 kA/cm^2). This output power was recorded by a power meter (Agilent 81636B). After accounting for a typical insertion loss of 5 dB,

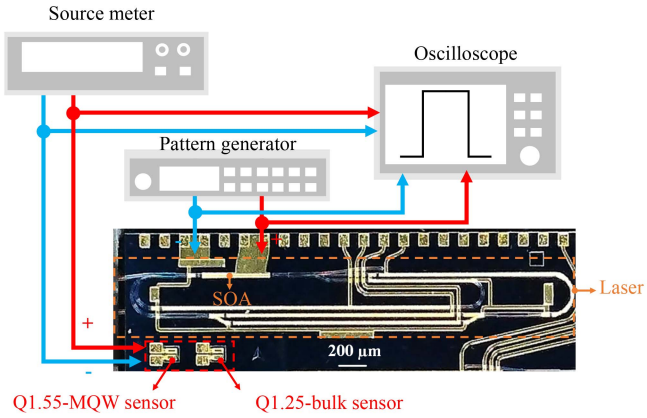

Fig. 7. Pulsed measurement setup and a microscope image showing the PIC housing the Q1.55-MQW sensor (left) and Q1.25-bulk sensor (right) that are co-integrated with a laser. The distance between the laser SOA and both sensors measures approximately 500 μm (core-to-core distance).

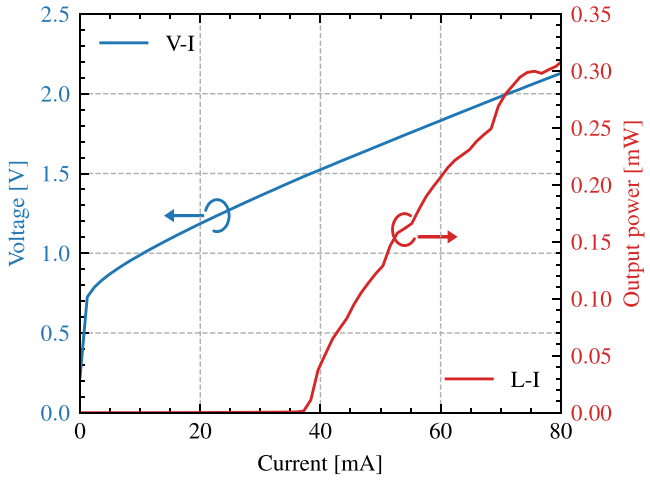

Fig. 8. Measurement results of the L-I-V characteristics of the laser, characterized at a stabilized temperature of 18 °C.

the optical power in the output waveguides was calculated to be 1 mW.

Pulsed measurements were performed at room temperature (22 °C) without the TEC enabled. The setup for the measurements is schematically depicted in Fig. 7. The Q1.55-MQW and Q1.25-bulk sensors, with a dimension of 60 × 20 μm, were forward-biased at the same constant current density of 0.8 A/cm^2 using a source meter (Keithley 2602B). The current density was chosen for the highest characterized sensitivity, −1.4 mV/K (Q1.55-MQW) and −2.1 mV/K (Q1.25-bulk), as shown in Table I. The forward-bias voltage of the sensor was monitored by an electrical oscilloscope (LeCroy LT584L), which was then converted to temperature change. The on-chip laser (integrated on the same PIC with the temperature sensors) was injected with current pulses with different frequencies, durations, and duty cycles under two different conditions: fast pulsing with rapid modulation (10 kHz with a 1 % duty cycle) and slow pulsing with slow modulation (1 Hz with a 50 % duty cycle). The pulses were generated by a pulse generator (Agilent 8114A), which

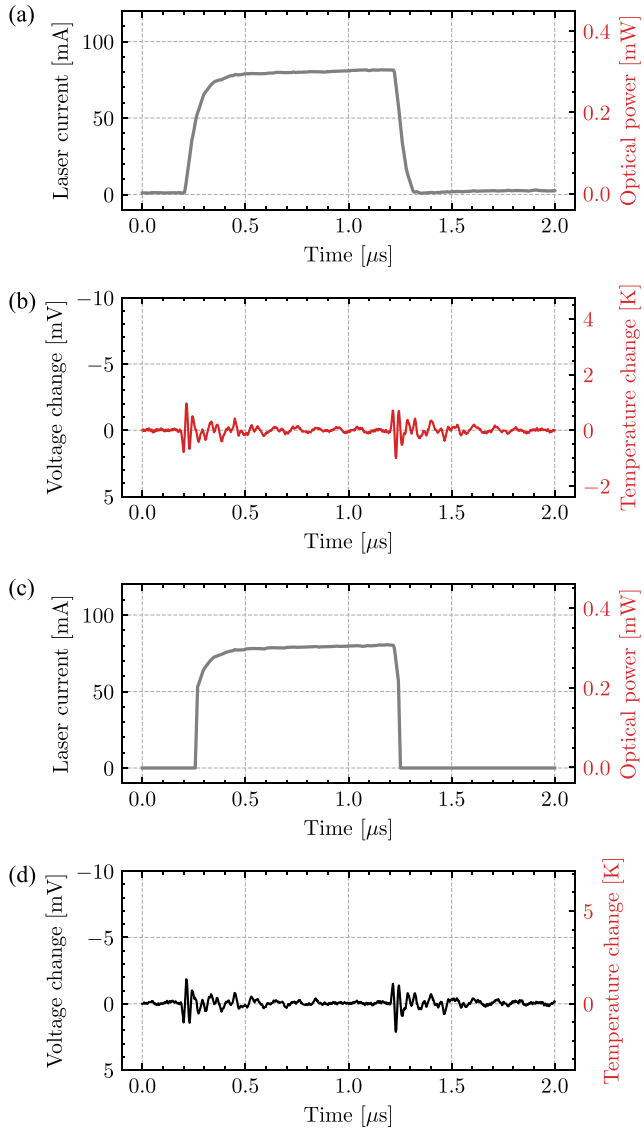

Fig. 9. Results of fast pulsing measurement for (a), (b) Q1.25-bulk and (c), (d) Q1.55-MQW temperature sensors within 2 μs and integration time of 10 ns. (a), (c): the current pulse (left axis) sent to the laser; and the output power from the laser (right axis) collected by an optical fiber. Note that: the pulses had a frequency of 10 kHz with a 1 % duty cycle, correlating to a pulse duration of 1 μs. (b), (d): the voltage change of the sensors (left axis) at a constant current density of 0.8 A/cm^2, with the derived temperature change (right axis).

was subsequently measured using the oscilloscope (LeCroy LT584L). The pulses were used to cyclically turn on and off the laser. The NTC thermistor, placed inside the chip holder as depicted in Fig. 4, was utilized as a reference temperature sensor to measure the temperature of the chip holder, indicating the overall temperature of the PIC.

Fig. 9 shows the results of the fast pulsing measurement. The laser was operated in a cyclical mode: a 1 μs activation duration, followed by a 99 μs deactivation phase, which formed a complete pulse cycle of 100 μs. This duty cycle was selected to allow enough cooling time (99 μs) after laser activation (1 μs), ensuring an effective reset of the on-chip temperature before the subsequent cycle. The current pulses applied to the laser had a peak amplitude at around 80 mA, as shown in Fig. 9(a) and

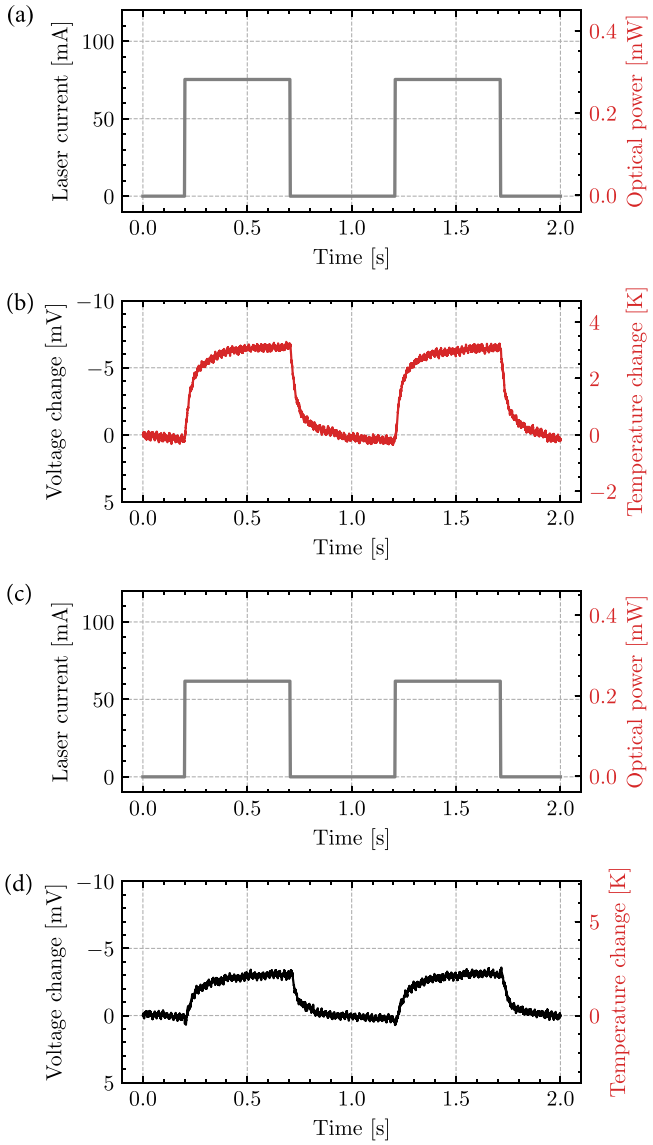

Fig. 10. Results of slow pulsing measurement for (a), (b) Q1.25-bulk and (c), (d) Q1.55-MQW temperature sensors within 2 s and integration time of 1 ms. (a), (c): the current pulse (left axis) sent to the laser; and the output power from the laser (right axis) collected by an optical fiber. Note that: the pulses had a frequency of 1 Hz with a 50 % duty cycle, correlating to a pulse duration of 0.5 s. The different amplitudes of the current pulses delivered to the on-chip laser shown in (a), (c) are attributed to differences in series resistance resulting from electrical wiring and probing between the two separate measurements, as the voltage was kept the same. (b), (d): the voltage change of the sensors (left axis) at a constant current density of 0.8 A/cm^2, with the derived temperature change (right axis).

(c). This current resulted in a laser power of 0.3 mW coupled in the optical fiber and 1 mW in the output waveguide, which was converted according to Fig. 8. During the pulse duration of 1 μs, the laser generates light and heat. Thermal transient simulations were conducted using the heat transfer module within the COMSOL Multiphysics simulation platform [34]. In the simulation, the cross-section of the SOA inside the laser cavity was constructed, the heat rate of the SOA was set to be 180 mW, somewhat higher than the electrical power used in the experiment. The thermal conductivity of the SOA core was assumed to be 5 W/mK, while the thermal conductivity of doped InP layers was assumed to be the same as InP ($\kappa_{\text{InP}} =$ 68 W/mK) [35]. Simulation results show that the measurement duration of 1 μs is significantly shorter than the heat dissipation from the laser SOA to the sensors (spaced at 500 μm). This is further confirmed by transient thermal analysis reported in [36]. Therefore, no heat but only stray light coming from the laser, will be present at the sensor in this measurement. As illustrated in Fig. 9(b) and (d), neither type of temperature sensor exhibited optically induced changes. High-frequency transient oscillations were observed in response to the pulse signal's rising and falling edges, and are attributed to electrical crosstalk in the wiring of the circuit. These oscillations can be minimized through appropriate shielding and design of the temperature sensor control circuit when implemented in a final application.

In contrast, notable temperature-dependent changes were observed in the forward voltages of the sensor during the slow pulsing measurement, as shown in Fig. 10. Here, the laser was injected with longer current pulses within an activation duration of 0.5 s. The duration was sufficiently long to enable heat dissipation from the laser to the sensors. This configuration enabled the laser to serve as both a light and heat source. Fig. 10(b) and (d) show that both sensors tracked the laser activation during slow pulsing, thereby capturing the heat dissipation and temperature fluctuations. Shown in Fig. 10(b), for instance, there was a voltage drop of 6 mV in the Q1.25-bulk sensor upon laser activation. This voltage drop corresponds to a temperature increase of approximately 3 K, calculated by dividing the 6-mV voltage reduction by the sensor's sensitivity of -2.1 mV/K. The off-chip NTC thermistor, located within the chip holder as depicted in Fig. 4, could not detect such rapid temperature changes.

V. Conclusion

This article presented for the first time integrated temperature sensing diodes in InP-based photonic integration technology. We studied two distinct types of (p-i-n) diodes, Q1.25-bulk and Q1.55-MQW, with different layer stacks. Their feasibility was assessed through theoretical analysis, simulations, and measurements. A linear relationship between temperature and voltage was observed in these sensors, with measured sensitivities ranging from -1.1 to -2.1 mV/K. The sensitivities are comparable to those of commercial temperature sensors in CMOS technology [15], [18]. The Q1.25-bulk sensors performed better than the Q1.55-MQW sensors, exhibiting higher sensitivities. Specifically, they achieved a measured sensitivity of $-$ 2.1 mV/K in a compact junction area of 10 $\times$ 30 μm. Their immunity to on-chip (stray) light was experimentally verified. Introducing these sensors into an InP-based generic foundry platform did not require any modification to the fabrication process. This indicates the general applicability of such sensors since only a diode structure is needed. Integrating multiple sensors, distributed at different locations in a PIC, would enable distributed temperature measurement and monitoring for accurate control of complex PICs.

ACKNOWLEDGMENT

The authors thank Yi Wang for fruitful discussions on the thermal management of photonic integrated devices. Ozan Çirkinoglu is acknowledged for laser design.

REFERENCES

[1] W. Yao, B. Smalbrugge, M. K. Smit, K. A. Williams, and M. J. Wale, "A 6×30 Gb/s tunable transmitter PIC with low RF crosstalk from an open-access InP foundry," *IEEE J. Sel. Topics Quantum Electron.*, vol. 25, no. 5, Sep./Oct. 2019, Art. no. 6100510.

[2] S. J. Ben Yoo, "Prospects and challenges of photonic switching in data centers and computing systems," *J. Lightw. Technol.*, vol. 40, no. 8, pp. 2214–2243, Apr. 2022.

[3] J. Sun, E. Timurdogan, A. Yaacobi, E. S. Hosseini, and M. R. Watts, "Large-scale nanophotonic phased array," *Nature*, vol. 493, no. 7431, pp. 195–199, 2013.

[4] L. A. Coldren, S. W. Corzine, and M. L. Mašanović, *Diode Lasers and Photonic Integrated Circuits*. Hoboken, NJ, USA: Wiley, 2012.

[5] P. Wen, P. Tiwari, M. Scherrer, E. Lörtscher, B. Gotsmann, and K. E. Moselund, "Thermal simulation and experimental analysis of optically pumped InP-on-Si micro- and nanocavity lasers," *ACS Photon.*, vol. 9, pp. 1338–1348, 2022.

[6] H. Li et al., "A 3-D-integrated silicon photonic microring-based 112-Gb/s PAM-4 transmitter with nonlinear equalization and thermal control," *IEEE J. Solid-State Circuits*, vol. 56, no. 1, pp. 19–29, Jan. 2021.

[7] L. Ranno et al., "Integrated photonics packaging: Challenges and opportunities," *ACS Photon.*, vol. 9, pp. 3467–3485, 2022.

[8] J. S. Lee et al., "Meeting the electrical, optical, and thermal design challenges of photonic-packaging," *IEEE J. Sel. Topics Quantum Electron.*, vol. 22, no. 6, pp. 409–417, Nov./Dec. 2016.

[9] K. Gradkowski et al., "Thermal challenges for packaging integrated photonic devices," in *Proc. IEEE 6th Electron. Syst.-Integration Technol. Conf.*, 2016, pp. 1–5.

[10] J. F. Tao, H. Cai, Y. D. Gu, J. Wu, and A. Q. Liu, "Demonstration of a photonic-based linear temperature sensor," *IEEE Photon. Technol. Lett.*, vol. 27, no. 7, pp. 767–769, Apr. 2015.

[11] L. Huang, J. Zhang, D. He, and X. Mi, "Dual-parameter optical sensor with cascaded ring resonators for simultaneous refractive index and temperature sensing," *Results Phys.*, vol. 43, 2022, Art. no. 106070.

[12] N. N. Klimov, S. Mittal, M. Berger, and Z. Ahmed, "On-chip silicon waveguide Bragg grating photonic temperature sensor," *Opt. Lett.*, vol. 40, no. 17, 2015, Art. no. 3934.

[13] H. Lu et al., "Integrated temperature sensor based on an enhanced pyroelectric photonic crystal," *Opt Exp.*, vol. 21, no. 14, pp. 16311–16318, 2013.

[14] S. M. Sze, Y. Li, and K. K. Ng, *Physics of Semiconductor Devices*. Hoboken, NJ, USA: Wiley, 2007.

[15] M. Mansoor, I. Haneef, S. Akhtar, A. De Luca, and F. Udrea, "Silicon diode temperature sensors–a review of applications," *Sensors Actuators A: Phys.*, vol. 232, pp. 63–74, 2015.

[16] G. C. M. Meijer, "Thermal sensors based on transistors," *Sensors Actuators*, vol. 10, no. 1, pp. 103–125, 1986.

[17] K. A. A. Makinwa, "Smart temperature sensors in standard CMOS," *Procedia Eng.*, vol. 5, pp. 930–939, 2010.

[18] F. Udrea, S. Santra, and J. W. Gardner, "CMOS temperature sensors - concepts, state-of-the-art and prospects," in *Proc. IEEE Int. Semicond. Conf.*, 2008, pp. 31–40.

[19] S. Jeong, Z. Foo, Y. Lee, J.-Y. Sim, D. Blaauw, and D. Sylvester, "A fully-integrated 71 nW CMOS temperature sensor for low power wireless sensor nodes," *IEEE J. Solid-State Circuits*, vol. 49, no. 8, pp. 1682–1693, Aug. 2014.

[20] C. Zhao, Y. T. Wang, D. Genzer, D. Chen, and R. Geiger, "A CMOS on-chip temperature sensor with -0.21°C 0.17°C inaccuracy from -20°C to 100°C," in *Proc. IEEE Int. Symp. Circuits Syst.*, 2013, pp. 2621–2625.

[21] G. C. M. Meijer, W. Guijie, and F. Fruett, "Temperature sensors and voltage references implemented in CMOS technology," *IEEE Sensors J.*, vol. 1, no. 3, pp. 225–234, Oct. 2001.

[22] A. McNamara, "Semiconductor diodes and transistors as electrical thermometers," *Rev. Sci. Instrum.*, vol. 33, no. 3, pp. 330–333, 1962.

[23] M. Kim et al., "Silicon electronic–photonic integrated 25 Gb/s ring modulator transmitter with a built-in temperature controller," *Photon. Res.*, vol. 9, no. 4, 2021, Art. no. 507.

[24] S. Saeedi and A. Emami, "Silicon-photonic PTAT temperature sensor for micro-ring resonator thermal stabilization," *Opt Exp.*, vol. 23, no. 17, pp. 21875–83, 2015.

[25] S. Yang et al., "Thermal stabilization of a microring resonator using bandgap temperature sensor," in *Proc. IEEE Opt. Interconnects Conf.*, 2015, pp. 44–45.

[26] C. T. DeRose, M. R. Watts, D. C. Trotter, D. L. Luck, G. N. Nielson, and R. W. Young, "Silicon microring modulator with integrated heater and temperature sensor for thermal control," in *Proc. Conf. Lasers Electro-Opt.*, 2010, Paper CThJ3.

[27] L. M. Augustin et al., "InP-based generic foundry platform for photonic integrated circuits," *IEEE J. Sel. Topics Quantum Electron.*, vol. 24, no. 1, pp. 1–10, Jan./Feb. 2018.

[28] M. Smit et al., "An introduction to InP-based generic integration technology," *Semicond. Sci. Technol.*, vol. 29, no. 8, 2014, Art. no. 083001.

[29] W. Tian et al., "Monolithically integrated temperature sensor in an InP-based generic integration technology," in *Proc. IEEE 26th Annu. Symp. Photon. Soc. Benelux Chapter*, 2022, pp. 58–61.

[30] W. Tian et al., "On-chip diode temperature sensors on InP-based generic foundry platform," in *Proc. IEEE 28th Opto-Electron. Commun. Conf.*, 2023, pp. 1–4.

[31] W. Shockley, "The theory of P-N junctions in semiconductors and P-N junction transistors," *Bell Syst. Tech. J.*, vol. 28, no. 3, pp. 435–489, 1949.

[32] "Hetero-structure laser diode model - Harold," Accessed: Aug. 2023. [Online]. Available: https://www.photond.com/products/harold.htm

[33] JePPIX. Accessed: Aug. 2023. [Online]. Available: https://www.jeppix.eu/

[34] "Heat transfer modeling software for analyzing thermal effects," Accessed: Dec. 2023. [Online]. Available: https://www.comsol.com/heat-transfer-module

[35] S. Adachi, *Physical Properties of III-V Semiconductor Compounds: InP, InAs, GaAs, GaP, InGaAs, and InGaAsP*. Hoboken, NJ, USA: Wiley, 1992.

[36] A. Gourevitch et al., "Transient thermal analysis of InGaAsP-InP high-power diode laser arrays with different fill factors," *J. Appl. Phys.*, vol. 97, no. 8, 2005, Art. no. 084503.